PHYSICAL REVIEW B **69**, 174503 (2004)

Critical parameters of disordered nanocrystalline superconducting Chevrel-phase $PbMo_6S_8$

H. J. Niu and D. P. Hampshire
Superconductivity Group, Department of Physics, University of Durham, Durham DH1 3LE, United Kingdom

(Received 23 June 2003; revised manuscript received 18 November 2003; published 21 May 2004)

Highly dense structurally disordered nanocrystalline bulk $PbMo_6S_8$ samples were fabricated by mechanical milling (MM) and hot isostatic pressing (HIP) at a pressure of 2000 bar and temperature of 800 °C for 8 h. In spite of the lower superconducting transition temperature ($T_C^{0.95\rho_N} = 12.3$ K), nanocrystalline bulk $PbMo_6S_8$ samples were found to have significantly higher resistivity $[\rho_N(16\,\mathrm{K}) = 680\ \mu\Omega\,\mathrm{cm}]$ and upper critical field $[B_{C2}^{M=0}(0) = 110\,\mathrm{T}]$ than conventional samples $[T_C^{0.95\rho_N} = 15.1\,\mathrm{K}$, $\rho_N(16\,\mathrm{K}) = 80\ \mu\Omega\,\mathrm{cm}$, and $B_{C2}^{M=0}(0) = 45$ T, respectively; Phys. Rev. Lett. **91**, 027002 (2003)]. The microstructural evolution during MM and HIP and the critical current density (J_C) are presented in this paper. J_C of the nanocrystalline bulk samples increased by a factor of more than 3 for high magnetic fields up to 12 T compared to the conventional sample. The scaling analysis is consistent with a grain-boundary pinning mechanism where $F_P \approx \{[B_{C2}^{J_C=0}(T)]^n/21\kappa^m\mu_0 d^*\}b^p(1-b)^q$ where $n\sim 2.35$, $m\sim 2$, $p\sim \frac{1}{2}$, $q\sim 2$, κ is the Ginzburg-Landau constant (calculated from reversible magnetization measurements), and d^* is the grain size (derived from x-ray diffraction analysis). Despite the pinning framework, the underlying science that determines J_C challenges the standard flux pinning paradigm that separates intrinsic and extrinsic properties, since the disorder and microstructure of these nanocrystalline materials are on a sufficiently short length scale as to increase both the density of (extrinsic) pinning sites and the (intrinsic) upper critical field.

DOI: 10.1103/PhysRevB.69.174503 PACS number(s): 74.70.−b, 81.07.Bc, 74.25.−q

I. INTRODUCTION

The Chevrel-phase superconductor $PbMo_6S_8$ has sufficiently high intrinsic properties to make it a potential material for the next generation of high-field magnets—the critical temperature (T_C) is ~15 K and the upper critical field (B_{C2})~50 T.[1] However, the values of critical current density (J_C) are too low for industrial use,[2] possibly because of degraded or nonsuperconducting phases, such as MoS_2 or Mo_2S_3, at the grain boundaries[3] or because the pinning site density is not high enough. It has long been known that decreasing the grain size of low-temperature superconducting (LTS) materials, such as Nb_3Sn, increases the density of flux pinning sites and hence J_C.[4–6] Such results have led to the flux pinning paradigm, used for ~40 yr, in which the microstructure determines the density and arrangement of the pinning sites and the material composition and electronic structure determines the fundamental superconducting properties. Increasing J_C can also increase the irreversibility field.[7] For example, in MgB_2, an increase in pinning led to an increase in the irreversibility field from $\sim 0.5B_{C2}$ up to $\sim 0.8B_{C2}$.[8] Since grain boundaries have also been identified as flux pinning centers in $PbMo_6S_8$,[9] one can expect that increasing the density of grain boundaries (e.g., producing nanocrystalline materials) will increase J_C and hence that control of grain size and atomic structure of grain boundaries is essential to achieve high J_C in high magnetic fields.[10]

Nanocrystalline materials are characterized by ultrafine grains and a high density of grain boundaries.[11] The grain boundaries of nanocrystalline materials may be different from those of conventional coarse grain materials and include equiaxed grain morphology, low-energy grain-boundary structures or flat grain-boundary configurations.[12] Hence nanocrystalline materials can exhibit unusual physical, chemical, and mechanical properties with respect to conventional polycrystalline materials.

High-energy impact during mechanical milling can be used to induce severe plastic deformation of milled metal and alloys to form nanocrystalline or amorphous powder.[13,14] Nanocrystallization of the amorphous powder can produce nanocrystalline materials with dense and clean grain boundaries, different types and levels of disorder, and/or nearly perfect crystallite structure through control of the heat treatment and thermomechanical processing.[15] This approach has been adopted to fabricate nanocrystalline and amorphous $PbMo_6S_8$ powder. The mechanical-milled $PbMo_6S_8$ powder was then subsequently annealed or hot isostatic pressed (HIP) to obtain the bulk samples. In a recent Letter,[16] we briefly reported that fabricating nanocrystalline superconductors provides a method to increase the upper critical field (B_{C2}) itself. For nanocrystalline $PbMo_6S_8$, B_{C2} can be ~110 T. The small grain size and high levels of disorder enhanced B_{C2} by increasing the resistivity (ρ_N) at the expense of decreasing T_C and the Sommerfeld constant (γ). Furthermore, the values of J_C found in zero field were the highest reported for bulk $PbMo_6S_8$. This paper includes a detailed analysis and discussion of the relationship between process parameters, microstructure, and superconducting properties, normal state electronic properties, and the role of strong electron-phonon coupling. Flux pinning in these highly disordered materials with very dense pinning is considered using the scaling laws.[17–20] The improvement in both J_C and B_{C2} in nanocrystalline materials challenges the flux pinning paradigm that separates the intrinsic superconducting properties from extrinsic properties, since the nanostructure and disorder increase both flux pinning and B_{C2}.

II. FABRICATION

$PbMo_6S_8$ powder was synthesized using elemental powders Pb (99.999%), S (99.998%), and Mo (99.95%). The Mo

TABLE I. Processing conditions, grain size (d), and lattice strain (ε) for the $PbMo_6S_8$ samples. The powder was heat treated at 1000 °C for 40 h before mechanical milling.

Sample	Milling (h)	HIP	Annealing	d (nm)	ε (%)
1	0			2000	0.00
2	100		800 °C×8 h	50	0.10
3	100		1000 °C×8 h	100	0.00
4	0	2000 bar, 800 °C×8 h		2000	0.00
5	200	2000 bar, 600 °C×8 h	1000 °C×40 h	90	0.02
6	200	2000 bar, 800 °C×8 h	1000 °C×10 h		
7	200	2000 bar, 800 °C×8 h	800 °C×40 h	30	0.04
8	200	2000 bar, 800 °C×8 h		20	0.07
9	200	2000 bar, 600 °C×8 h	600 °C×40 h	20	0.13
10	200	2000 bar, 600 °C×8 h		10	1.32

powder was reduced under pure H_2 gas flow at 1000 °C for 4 h. The details of the fabrication and heat treatments have been described previously.[21] The final heat treatment to produce the starting $PbMo_6S_8$ material was 1000 °C for 40 h.

The sintered $PbMo_6S_8$ powder (5 g) was put into a Syalon pot and mechanically milled for up to 200 h at a rotational velocity of 300 revolutions per minute (rpm) using six Syalon balls with a diameter of 20 mm. The weight ratio of the Syalon balls to the powder was ~16:1. Mechanical milling was carried out in a steel box under Ar gas flow. The powder milled for 100 h was subsequently sintered at temperatures of 800 and 1000 °C for 8 h. The 200 h milled powder was wrapped inside Mo foil and sealed in a stainless steel tube and then HIP at a pressure of 2000 bar and temperatures of 600 and 800 °C for 8 h. Some of the HIP samples were subsequently annealed at temperatures of 600, 800, and 1000 °C for 40 h. The details of the processing conditions are listed in Table I. Samples 1–3 are the sintered samples used to investigate phase transformations and the superconducting transition during annealing. Sample 4 is a conventional HIP sample. The HIP samples (4–10) are labeled with increasing numbers to broadly indicate the increased disorder and smaller grain size associated with progressively less recovery/crystallization produced by the HIP/annealing after milling.

X-ray diffraction (XRD) was performed using PW1800 and Siemens D5000 powder diffractometers. A high-resolution S4000 FE scanning electron microscope (SEM) was used to investigate powder morphology. Differential scanning calorimetry (DSC) and thermogravimetry (TG) were carried out on a Netzsch STA from 400 to 1100 °C at 20 °C/min.

III. RESULTS AND DISCUSSION

A. Microstructure

Figure 1 shows XRD patterns of $PbMo_6S_8$ powder mechanically milled for up to 200 h, together with an equivalent XRD pattern of as-sintered $PbMo_6S_8$ powder. The as-sintered powder is single-phase $PbMo_6S_8$. With increasing mechanical milling time, the XRD peaks broadened due to decreasing grain size and increasing lattice strain. Prolonged milling for 200 h leads to the formation of very broad peaks due to the presence of amorphous material, although some small peaks from crystalline $PbMo_6S_8$ are still visible. The particle morphologies of mechanically milled $PbMo_6S_8$ powder are shown in Fig. 2. The powder milled for 5 h had a wide range of particle sizes, while the powder milled for 30 h had a more uniform and smaller particle size. A slight decrease in the particle size was found with further increase in milling time to 200 h. Figure 3 shows that the hexagonal lattice parameters (c,a) of $PbMo_6S_8$ remained almost constant for milling times up to 15 h, while the large particles were simply fractured into small ones. A gradual increase in the lattice parameters probably due to inducing defects, such as vacancies, into the particles followed with further increase in milling time to 100 h. A rapid increase in lattice parameters with increasing milling time from 100 to 200 h was found, probably due to the supersaturation of vacancies in the lattice as reported in other materials with a grain size of several nanometers.[22] The mixed structure of very small grains (~10 nm) and amorphous material in the 200 h milled powder is consistent with the small grain size calculated from the XRD results and transmission electron microscopy reported previously.[23]

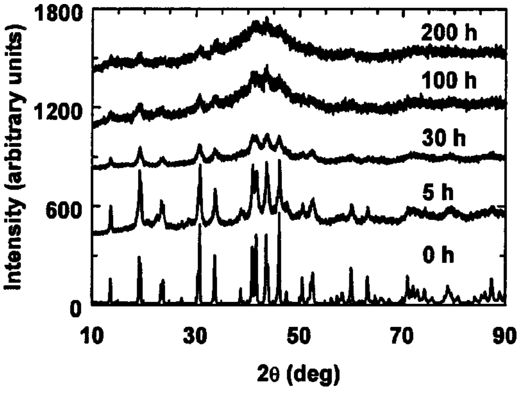

FIG. 1. XRD patterns of $PbMo_6S_8$ powders mechanically milled for up to 200 h.

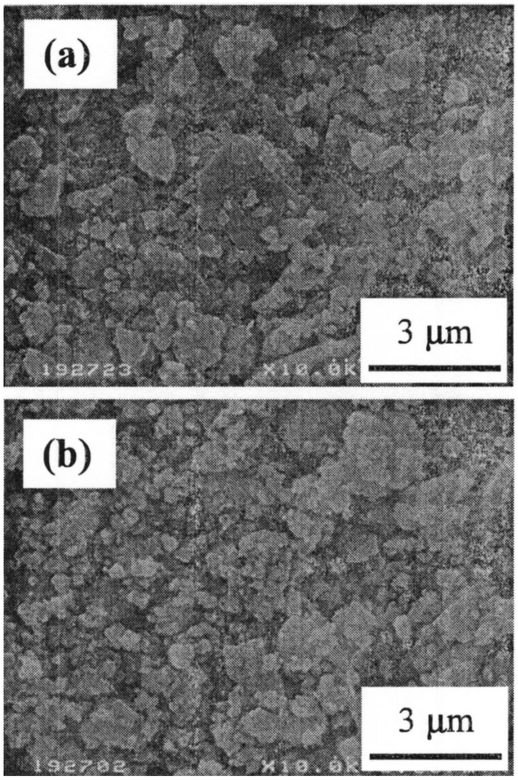

FIG. 2. SEM micrographs of the mechanically milled $PbMo_6S_8$ powders: (a) 5 and (b) 200 h.

Figure 4 shows the DSC and TG traces of the powders milled for 100 and 200 h at a heating rate of 20 °C min^{-1}. Two exothermic reactions were found in the DSC scan in the temperature range between 400 and 900 °C, as shown in Fig. 4(a). The first DSC dip was a broad exothermic valley, with an onset temperature at ~440 °C and a minimum at about 600 °C. The exothermic heat is attributed to the recovery of lattice strain and growth of the nanocrystalline phase and is consistent with the XRD described below. Similar exothermic peaks have also been observed in a mechanically milled YNi_2B_2C superconductor[24] and a $Ni_{81}P_9$ alloy.[25] The second DSC dip was in the temperature range from 680 to 800 °C, which corresponds to about $0.5T_m$ (T_m is the melting temperature in kelvin). This exothermic peak probably arises from the crystallization of the amorphous phase. The temperature interval of this peak is close to that of the exothermic peak produced during the synthesis of $PbMo_6S_8$.[26] Prolonged mechanical milling increases the proportion of amorphous material in the mixed structure. Therefore, one can expect the powder milled for 100 h to release more energy during recovery and growth of the nanocrystalline phase but less energy during the crystallization of the amorphous phase than that milled for 200 h, as shown in Fig. 4(a). The TG traces [Fig. 4(b)] show that the mass decreased with increasing temperature, particularly at the temperature of the second exothermic peak. It is believed that evaporation of S

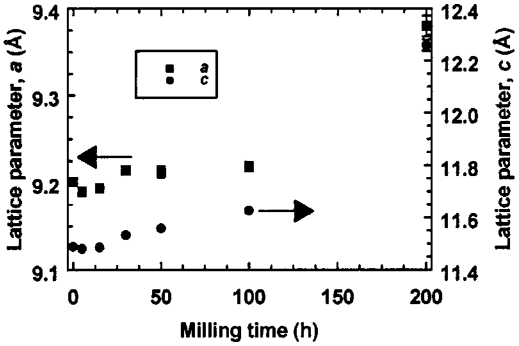

FIG. 3. Variation of the hexagonal lattice parameters (*a*,*c*) of $PbMo_6S_8$ with mechanical milling time.

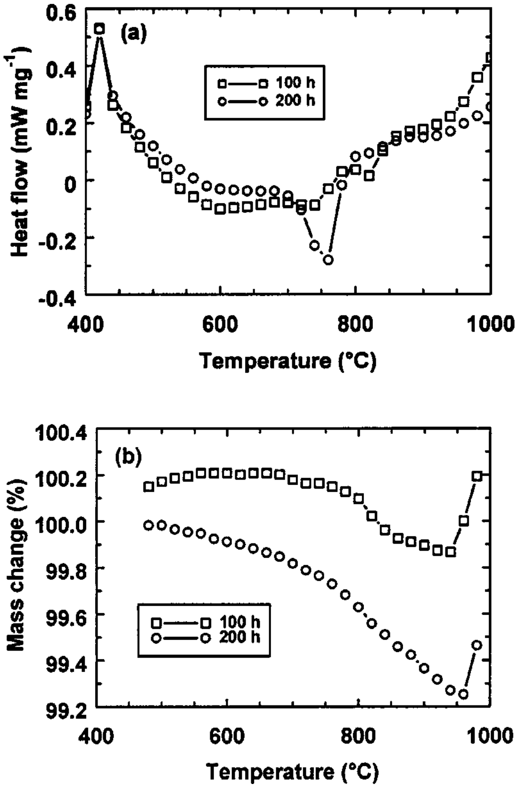

FIG. 4. Thermal analysis of $PbMo_6S_8$ powders mechanically milled for 100 and 200 h: (a) differential scanning calorimetry (DSC); (b) thermogravimetry (TG).

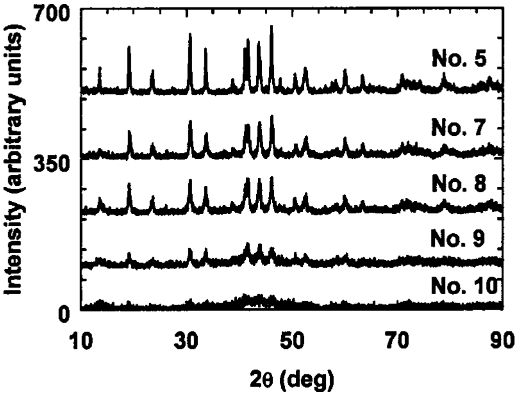

FIG. 5. XRD patterns for the $PbMo_6S_8$ samples HIP and annealed for different temperatures and times. The powder was mechanically milled for 200 h before HIP.

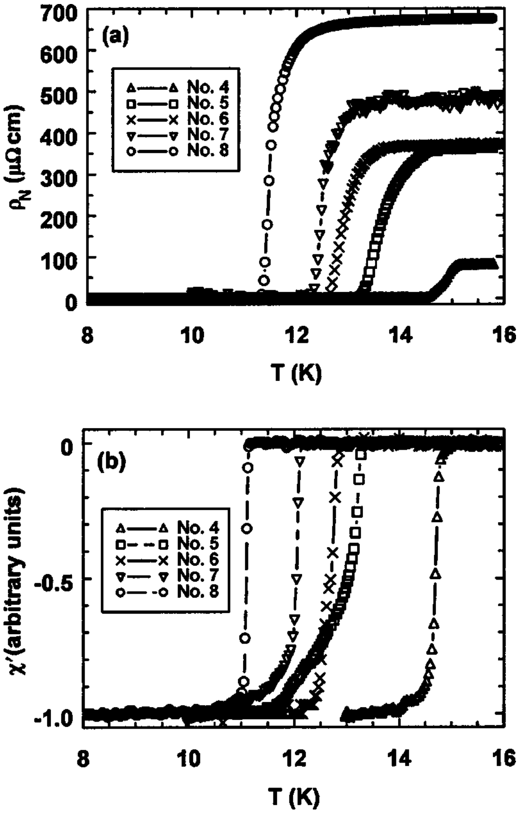

FIG. 6. The resistivity (a) and lossless susceptibility (b) versus temperature of the HIP $PbMo_6S_8$ samples.

and Pb during heating caused the mass loss. The powder milled for 200 h lost more mass, probably because it had more amorphous material and smaller particle size. Above 800 °C, a higher atomic mobility during crystallization enhances mass loss. Above 950 °C, oxidation of the powders caused the mass increase.

Figure 5 shows the XRD patterns of the milled and HIP samples. A systematic decrease in the width of the XRD peaks is observed with increasingly aggressive heat treatment (i.e., longer temperature and longer time). The XRD peaks of the $PbMo_6S_8$ phase are faint for the milled powder HIP at 600 °C for 8 h, because the amorphous phase has not yet crystallized. The sample incorporated a small grain size (10 nm) but a very large strain (1.32%), determined using the Hall-Williamson method[27] in which

$$\frac{F\cos\theta}{\lambda}=\frac{1}{d}+\frac{4\varepsilon\sin\theta}{\lambda}, \tag{1}$$

where F is the difference of the full width at half maximum (FWHM) between the milled sample and the sintered sample, d is the crystallite size, ε is the lattice strain, and θ is the Bragg angle (Table I). Broad $PbMo_6S_8$ XRD peaks appeared after subsequently annealing at the same temperature for 40 h. HIP at 800 °C for 8 h led to relatively sharp peaks of the $PbMo_6S_8$ phase due to the complete crystallization of amorphous phase and the increased grain size (20 nm). Annealing at 800 °C for 40 h produced no obvious change in the XRD pattern although annealing at 1000 °C for 40 h significantly sharpened the XRD peaks and increased the grain size (90 nm). However, the HIP and annealed samples had much smaller grain sizes (<100 nm) than the conventional sample (~2 μm). In addition, optical microscopy confirms that the nanocrystalline material is significantly more dense than conventional material.

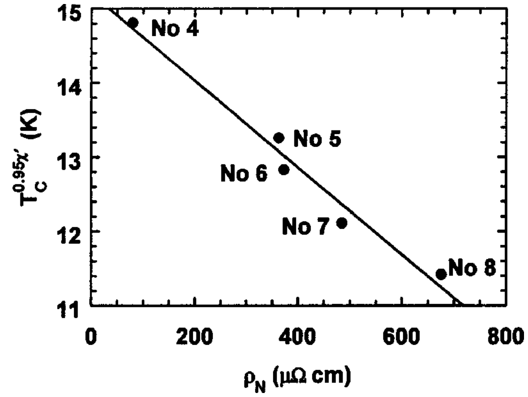

FIG. 7. Variation of critical temperature ($T_C^{0.95\chi'}$) with normal state resistivity (ρ_N) at 16 K for the $PbMo_6S_8$ samples.

B. Critical parameters

Susceptibility and resistivity measurements were used to determine T_C of the HIP and annealed samples, as shown in Fig. 6. Increasing postannealing temperature and time increased T_C measured by both resistivity and susceptibility. A clear correlation between increasing ρ_N and decreasing T_C, shown in Figs. 6 and 7, can be attributed to a decrease in disorder with increased annealing temperature and time. The T_C values obtained in these HIP and annealed nanocrystalline samples are still lower than those in the conventional sample, indicating they are not fully recovered large grain material. In general, the onset of the superconducting transition measured by resistivity characterizes the grains with the highest critical superconducting properties, whereas the onset determined by susceptibility measurement is lower since it requires the grain boundaries to be superconducting.[28] The transition width was ~0.5 K from both the resistivity and susceptibility measurements for the conventional sample 4

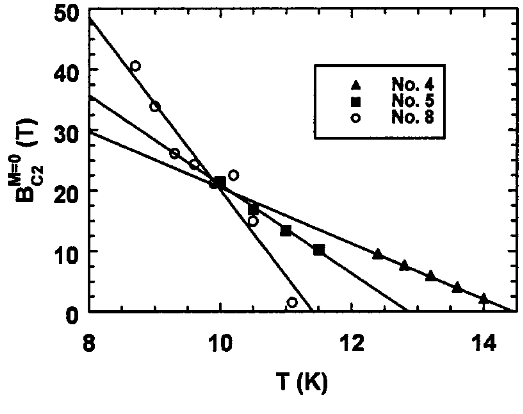

FIG. 8. Variation of the upper critical field ($B_{C2}^{M=0}$) with temperature (T) for samples 4, 5, and 8.

TABLE II. Normal state resistivity (ρ_N), residual resistivity ratio (RRR), and superconducting parameters of HIP $PbMo_6S_8$ samples. The Ginzburg-Landau parameter κ_2 was calculated from the gradient of the reversible magnetization data using the Abrikosov equation (Ref. 58) $\mu_0 M = -(B_{C2}-B)/(2\kappa_2^2-1)\beta_A|_{B_{C2}}$, where $\beta_A = 1.16$. The parameters in this table do not depend on the strength of the electron-phonon coupling.

Sample	ρ_N (16 K) ($\mu\Omega$ cm)	RRR	$T_C^{0.95\rho_N}$ (K)	$-dB_{C2}^{M=0}/dT$ (T K^{-1})	$T_C^{M=0}$ (K)	$B_{C2}^{M=0}$ (T)	κ_2	$\xi(0)$ (nm)	$\lambda(0)$ (nm)	$B_{c1}(0)$ (mT)
4	80	7.8	15.1	4.6	14.4	45	125	2.2	275	5.8
5	360	2.0	14.4	7.3	12.9	65	240	1.9	455	2.0
8	680	1.4	12.3	14.1	11.5	110	520	1.4	745	1.0

and equivalent values of ~1.0 and ~0.2 K were found for sample 8. This indicates that the nanocrystalline sample is inhomogeneous but the grain boundaries are similar throughout.

The linear relation in Fig. 7 between increasing $T_C^{0.95\chi'}$ and decreasing ρ_N gives $\rho_N = 2.6\ \mathrm{m}\Omega\,\mathrm{cm}$ at $T_C^{0.95\chi'} = 0$, which is similar to 1.2 $\mathrm{m}\Omega\,\mathrm{cm}$ obtained for the HTS $Bi_2Sr_2Y_xCa_{1-x}Cu_2O_8$ when the yttrium content drove T_C to zero.[29] Similar behavior has also been found in HTS materials as a function of oxygen content,[30,31] in $EuMo_6S_8$ when pressure is applied[32] and in films of Bi.[33] The decrease in T_C with increasing ρ_N may be in part due to decreasing electronic density of states at the Fermi surface[34] but the phonon spectrum, which is usually softened in the nanocrystalline materials,[35] may also play a role since, for example, in BCS superconductors such softening would tend to increase T_C.[36] However, at present there can be no detailed understanding of the widespread behavior typified in Fig. 7 without understanding the microscopic mechanism that causes superconductivity. The concern is that the well-known Uemura plot[37] suggests that HTS materials and Chevrel-phase materials have a similar mechanism causing superconductivity although BCS theory works well for Chevrel-phase materials which are close to the metal-insulator transition whereas it does not for the HTS materials.[38]

Figure 8 and Table II show the markedly higher $B_{C2}^{M=0}(0)$ from the reversible magnetization measurements in the nanocrystalline materials compared to conventional materials and reported in the previous Letter.[16] The calculated values for the Sommerfeld constant γ and the temperature dependence of the thermodynamic critical field, $B_C(T)$, are significantly affected by whether or not $PbMo_6S_8$ is strongly coupled. In the strong coupling limit, Marsiglio and Carbotte[39] found

$$-\left(\frac{dB_C(T)}{dT}\right)\bigg|_{T_C} = 1.20\mu_0^{1/2}\gamma^{1/2}\left\{1+53\left(\frac{T_C}{\omega_{\ln}}\right)^2\ln\left(\frac{\omega_{\ln}}{3T_C}\right)\right\}^{1/2} \tag{2}$$

and

$$\frac{\mu_0\gamma T_C^2}{B_C^2(0)} = 2.11\left\{1-12.2\left(\frac{T_C}{\omega_{\ln}}\right)^2\ln\left(\frac{\omega_{\ln}}{3T_C}\right)\right\}. \tag{3}$$

Although strong electron-phonon coupling is well established in some Chevrel-phase compounds,[40] there are conflicting results reported for $PbMo_6S_8$ showing both weak[41] and strong[42,43] coupling where $\omega_{\ln}$ is ∞ and 185 K, respectively. These differences are probably due to the different processing conditions and sulfur content of samples in the literature. In this context, we note that $T_C^{0.95\rho_N} = 15.1$ K for the conventional sample is equal to the highest reported in the literature.[44] The values of $B_C(0)$ and γ have been calculated for both these limits and shown in Table III. Since the values of $B_C(0)$ for both the conventional and nanocrystalline samples are similar, it confirms that the high $B_{C2}^{M=0}$ values are bulk properties. Despite the strongly sample-dependent properties reported in the literature, since the calculated value of γ for $\omega_{\ln} \sim 185$ K is closest to the value obtained from specific heat[33] (250 $\mathrm{J\,K^{-2}\,m^{-3}}$) these materials are probably strongly coupled. Nevertheless, the increase in $B_{C2}^{M=0}(0)$ found in the nanocrystalline materials is explained by the decrease in γ (whether strongly coupled or not) and T_C being more than compensated for by the rapid increase in ρ_N from 80 to 680 $\mu\Omega$ cm. Since the values of $\xi(0)$ (1.4 nm) are more than an order of magnitude smaller than the grain

TABLE III. Thermodynamic critical field at zero temperature $[B_C(0)]$ and the Sommerfeld constant (γ) of HIP $PbMo_6S_8$ samples obtained from reversible magnetization measurements. The weighted average phonon frequencies $(\omega_{\ln})$ are ∞ and 185 K for the weak and strong coupling limits, respectively.

	$\omega_{\ln} = \infty$		$\omega_{\ln} = 185$	
Sample	$B_C(0)$ (T)	γ ($\mathrm{J\,K^{-2}\,m^{-3}}$)	$B_C(0)$ (T)	γ ($\mathrm{J\,K^{-2}\,m^{-3}}$)
4	0.22	380	0.19	265
5	0.16	250	0.14	180
8	0.13	200	0.11	150

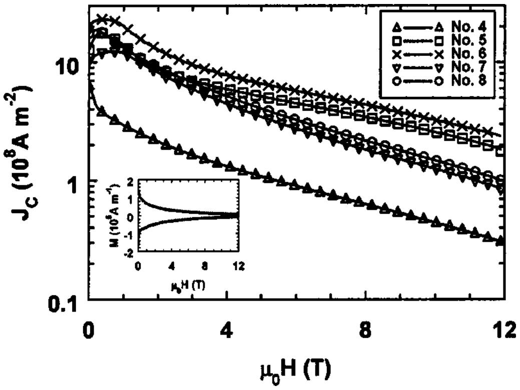

FIG. 9. Variation of critical current density (J_C) of $PbMo_6S_8$ samples with magnetic field at 4.2 K for samples 4, 5, 6, 7, and 8. Inset: *M-H* curve of sample 4 measured using a commercial vibrating-sample magnetometer at a temperature of 4.2 K and magnetic field up to 12 T.

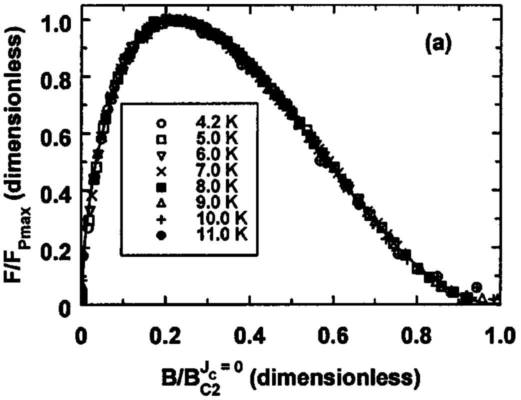

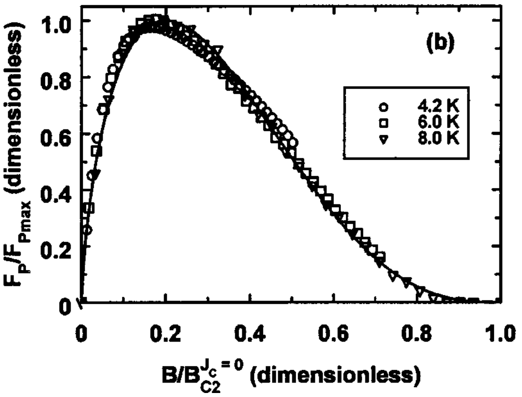

FIG. 10. Variation of normalized pinning force with normalized field for $PbMo_6S_8$: (a) sample 4; (b) sample 8.

size, a significant contribution to the increase in resistivity must be due to a high level of disorder and strain in the nanocrystalline grains.

C. Critical current density

Figure 9 shows the variation in J_C for the HIP samples taken in magnetic fields up to 12 T at the temperature of 4.2 K. J_C was calculated for these rectangular samples using the relation[19,45]

$$J_C = \frac{\Delta M}{a_2(1 - a_2/3a_1)}, \tag{4}$$

where ΔM is the difference in hysteretic magnetization for increasing and decreasing fields (cf. the inset in Fig. 9), and $2a_1$ and $2a_2$ ($a_1 \geqslant a_2$) are the width and thickness of the samples, respectively.

The nanocrystalline samples have J_C values that are a factor of above 3 higher than the conventional sample in high fields up to 12 T. Annealing at 1000 °C after HIP produces a markedly higher J_C in fields above 4 T. The values of J_C at 5 T and 4.2 K are from 5.0 to 6.5×10^8 A m^{-2} for the high-temperature-annealed samples. These values are higher than 4.8×10^8 A m^{-2} measured on the hot pressed $PbMo_6S_8$ sample after irradiating with fast neutrons at room temperature[46] and to our knowledge the highest reported for bulk pellet samples in the literature.

The volume pinning force is now considered within a very general framework for the scaling law[5,17]

$$F_P = J_C \times B = A\frac{[B_{C2}^{J_C=0}(T)]^n}{\kappa^m} b^p (1-b)^q, \tag{5}$$

where b is the reduced field $B/B_{C2}^{J_C=0}$, n, m, p, and q are constants depending on the pinning mechanism, and A is a constant dependent on extrinsic parameters such as the microstructure. This scaling law can describe the magnetic field, temperature, and strain dependence of J_C in some low-temperature superconductors such as A15 compounds when the temperature and strain dependence of κ is included.[20,47] The reduced volume pinning force ($F_P/F_{P_{\max}}$) versus the reduced magnetic field (b) is plotted as a function of temperature and shown in Fig. 10. The peak values of $F_P/F_{P_{\max}}$ is at $b \approx 0.23$ for the conventional sample and $b \approx 0.20$ for the HIP nanocrystalline sample, suggesting that the pinning force broadly follows the Kramer relation.[48,49] However, the $F_P/F_{P_{\max}}$ peaks tend to be sharper and shift to lower b values with increasing level of disorder. In Table IV, the values of $B_{C2}^{J_C=0}$ at 4.2 K determined from fitting the data to Eq. (5) are shown. The values of $B_{C2}^{J_C=0}$ are much smaller than $B_{C2}^{M=0}$. A simple explanation is that $B_{C2}^{J_C=0}$ is characteristic of the degraded local properties at the grain boundaries.[2,50] Figure 11 shows the linear relationship between log($F_{P_{\max}}$) and log($B_{C2}^{J_C=0}$) required to determine an accurate value for the exponent n. Table IV also lists the values of A, n, and $p/(p+q)$ calculated using Eq. (5) following Fietz and Webb[51] and the grain size. Theoretical considerations of grain-boundary pinning, including flux shear along grain boundaries, suggest $A \approx 1/21\mu_0 d^*$, $n=2$, and $m=2$.[6,52] Indeed, a simple dimensionality argument suggests that $n=2$, if it is assumed that $F_P \propto 1/d^*$.[4] In Table IV, values for d^* are shown that have been calculated using these constraints and κ_2 derived from the reversible magnetization data. The values for d^* are in reasonably good agreement with the grain sizes determined by XRD analysis consistent with grain boundary pinning.[6,52]

TABLE IV. Scaling parameters $B_{C2}^{J_C=0}$ (4.2 K), A, n, and $p/(p+q)$ obtained from Eq. (5), and the grain size (d^* and d) and κ_1 calculated from Eq. (6). κ_2 is taken as the average value from the reversible magnetization measurements, d^* was calculated assuming $A \approx 1/21\mu_0 d^*$, $m=2$, $n=2$, $p=0.5$, $q=2$, and d was obtained from the structural analysis.

Sample	$B_{C2}^{J_C=0}$ (4.2 K) (T)	$A(m=2,\kappa_2)$ (10^8 A m^{-2} T$^{(n-1)}$)	n	$p/(p+q)$	d^* (nm)	d (nm)	κ_1 (4.2 K)
4	24	225	2.3	0.23	1550	2000	123
5	29	2 500	2.4	0.22	138	90	195
7	24	12 300	2.5	0.20	28	30	275
8	24	36 000	2.2	0.20	10	20	205

The relatively low values of $B_{C2}^{J_C=0}$ suggest finding a complementary local value for the Ginzburg-Landau parameter at the grain boundaries may be required in any self-consistent description. Ginzburg-Landau theory provides an empirical relation for determining κ_1 as follows:

$$\kappa_1(T) = \frac{B_{C2}^{J_C=0}(T)}{\sqrt{2}B_C(T)} = 1.03\frac{B_{C2}^{J_C=0}(T)}{\mu_0^{1/2}\gamma^{1/2}T_C(1-t^2)} \times\left[1-12.2\left(\frac{T_C}{\omega_{\ln}}\right)^2 \ln\left(\frac{\omega_{\ln}}{3T_C}\right)\right]^{1/2}, \tag{6}$$

where $t=T/T_C$. Using the γ values from the strong coupling regime in Table III, the values of κ_1 at different temperatures were calculated using Eq. (6). Table IV shows values of κ_1 at 4.2 K, which are lower than those of κ_2 from the magnetization data. The fits to Eq. (5) using κ_1 give relatively large values of n (2.6–2.9) but small values in A and thus very large grain size in comparison to those calculated using κ_2. Hence, within the flux pinning framework, the best fit to the data is consistent with grain-boundary pinning, where the upper critical field is left as a free fitting parameter and the Ginzburg-Landau parameter is taken to be independent of temperature and obtained from the reversible magnetization data.

Despite the good agreement between the grain-boundary pinning model and the data, one should also consider non-scaling descriptions of these data, where the quality or thickness of the grain boundaries is considered.[53] Evidence for the importance of the properties of grain boundaries comes from the increase in $B_{C2}^{J_C=0}$ by 5 T at 4.2 K after high-temperature annealing at 1000 °C as shown in Table IV. Improved superconducting properties at the grain boundaries explain the increase in J_C above 4 T (shown in Fig. 9) following high-temperature annealing after HIP. Further improvement in superconducting properties at the grain boundary in these nanocrystalline samples can be expected by optimizing the heat treatment process or doping at the grain boundaries. This section now considers the pinning description and some alternative explanations. Instead of a pinning function [Eq. (5)], the magnetic field dependence of the J_C data in Fig. 9 can clearly be parametrized using an exponential form. It has long been known that many high-temperature superconductors can show a similar exponential field dependence.[54,55] If over the field range available for measurement J_C changes by less than two orders of magnitude, it is very difficult to distinguish an exponential form from a Kramer pinning function.[56] The interpretation of $B_{C2}^{J_C=0}$, in the pinning description, is the characteristic magnetic field that delineates the superconductivity from the normal state. As part of the exponential form, $B_{C2}^{J_C=0}$ becomes the characteristic magnetic field over which J_C decays to about 1% of the low magnetic field values of J_C,[56] and one would not expect J_C to be zero when $B > B_{C2}^{J_C=0}$. Therefore, given that the exponential fall for all samples in Fig. 9 is similar, one may expect that the values of $B_{C2}^{J_C=0}$ shown in Table IV are similar for all the samples. Indeed, there is no evidence in the data for a phase transition at $B_{C2}^{J_C=0}$. Even J_C data taken at higher temperature where an apparent irreversibility field is measured when the hysteresis drops to less than the noise floor in the vibrating-sample-magnetometer (VSM) measurements has to be interpreted with care. It has been demonstrated that when VSM measurements are reversible, J_C is not necessarily zero; rather the self-field produced by pinning in the sample is of the same magnitude as the ac field the sample experiences while it oscillates during the VSM measurement.[57]

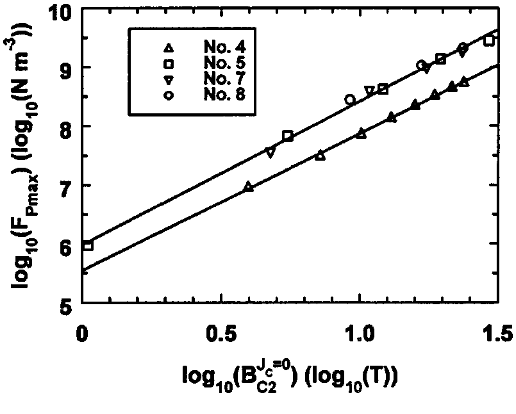

FIG. 11. Variation of maximum pinning force $\log_{10}(F_{P_{\max}})$ with $\log_{10}(B_{C2}^{J_C=0})$ for samples 4, 5, 7, and 8.

Without prejudging the field dependence of the J_C data, the form of the maximum value of F_P (i.e., $F_{P_{\max}}$), is now considered. If the form for F_P does not explicitly introduce a

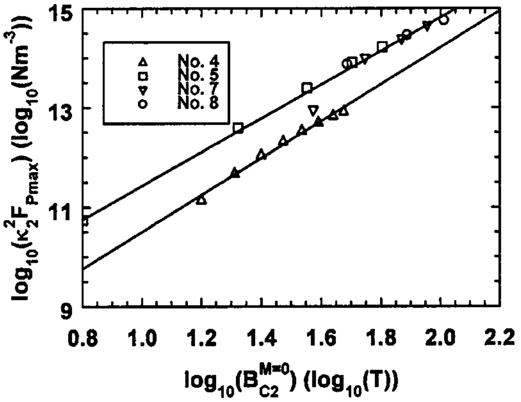

FIG. 12. Variation of maximum pinning force $\log_{10}(\kappa_2^2 F_{P_{\max}})$ with $\log_{10}(B_{C2}^{M=0})$ for samples 4, 5, 7, and 8.

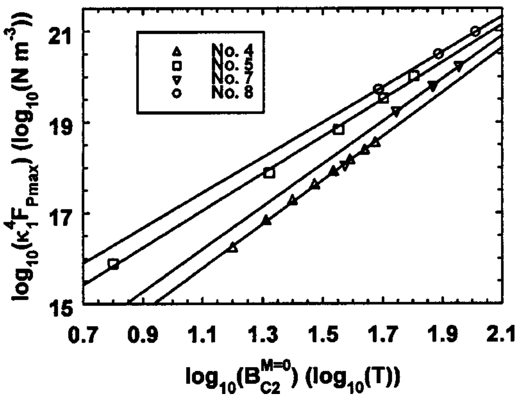

FIG. 13. Variation of maximum pinning force $\log_{10}(\kappa_1^4 F_{P_{\max}})$ with $\log_{10}(B_{C2}^{M=0})$ for samples 4, 5, 7, and 8.

scaling or irreversibility field, the natural choice for the scaling field becomes $B_{C2}^{M=0}$ determined from the magnetization data. Consider

$$F_{P_{\max}} = A^* \left(\frac{(B_{C2}^{M=0}(T))^n}{\kappa^m} \right). \tag{7}$$

In Fig. 12, $\log(\kappa_2^m F_{P_{\max}})$ versus $\log(B_{C2}^{M=0})$ is plotted for $m = 2$. Alternatively, a temperature dependence for κ_1 can be included through Eq. (6). Figure 13 is a log-log plot of $\kappa_1^4 F_{P_{\max}}$ versus $B_{C2}^{M=0}$ which shows good linearity for all the samples. Detailed analysis of these very different approaches for considering Eq. (7) shows that the data for the conventional and nanocrystalline $PbMo_6S_8$ samples can be parametrized rather well with either κ_1 or κ_2 with values for m over the range 0–4. The equivalent n values are typically about 4 compared to values of about 2 for the pinning description.

In summary, a comprehensive analysis of the pinning force in these high-J_C nanocrystalline materials shows that a scaling law gives a good parametrization of the J_C data, which agrees with phenomenological calculations in which the grain size has been calculated from XRD data and the Ginzburg-Landau parameter from reversible magnetization data. The important free parameter is $B_{C2}^{J_C=0}$, which has to be added in an *ad hoc* way, but can be interpreted as an irreversibility field or as the local value of the upper critical field at the grain boundaries. If κ is taken to be temperature independent, the values of n are ~2.25, which is significantly higher than the value 2 from theory. If a temperature dependence of κ is introduced using Eq. (6), the experimental value of n increases, so the difference between n in grain-boundary pinning theory (i.e., $n=2$) and experiment is larger, as has also observed in Nb_3Sn and Nb_3Al.[20,47] A nonscaling approach has also been considered. When the maximum volume (pinning) force is parametrized in terms of $B_{C2}^{M=0}$ using Eq. (6), although a broad range of m values fit the data, the values of n are high, typically about 4. Further development of scaling/nonscaling models and measurements of the local upper critical field are required to understand these high values of n in Chevrel-phase materials.

IV. CONCLUSIONS

Amorphous and nanocrystalline $PbMo_6S_8$ powders were produced by mechanical milling for up to 200 h. HIP of the milled powder at a pressure of 2000 bar produces highly dense nanocrystalline bulk samples (10–100 nm) with structural disorder. A strongly disordered nanocrystalline bulk $PbMo_6S_8$ sample has a significantly higher $B_{C2}^{M=0}(0)$ value than conventional $PbMo_6S_8$ samples. The increase in $B_{C2}^{M=0}(0)$ is due to the decrease in γ and T_C being more than compensated for by the rapid increase in ρ_N.

J_C of the disordered nanocrystalline bulk samples increases by a factor of above 3 for high magnetic fields up to 12 T compared to the conventional sample, although $B_{C2}^{J_C=0}(T)$ values are typically half the thermodynamic upper critical field ($B_{C2}^{M=0}$) determined from reversible magnetization measurements. Scaling analysis reveals that the increase in J_C in nanocrystalline materials can be attributed to the increase in flux pinning centers. High-temperature annealing at 1000 °C for 40 h decreases flux pinning centers due to decreasing structural disorder but improves $B_{C2}^{J_C=0}(T)$ at the grain boundary, by about 5 T at 4.2 K, which leads to an increase in J_C with increasing magnetic field. The grain sizes determined from scaling agree remarkably well with those calculated from XRD analysis.

If no assumptions are made as to whether scaling operates, the empirical law $F_{P_{\max}} = A^*[(B_{C2}^{M=0}(T))^n/\kappa^m]$ describes the data where $n \sim 3-5$ whether κ is taken from magnetization measurements or a Ginzburg-Landau relation. Further development of scaling/nonscaling models (which abandon the standard flux paradigm) and measurements of the local upper critical field are required to understand the exponents n and m in nanocrystalline Chevrel-phase materials with very high upper critical field.

ACKNOWLEDGMENTS

We would like to thank Dr. J. S. O. Evans for the XRD measurement and Dr. C. Li for the SEM analysis. This work was supported by EPSRC U.K. Grant No. GR/M85517.

[1] Ø. Fischer, Appl. Phys. **16**, 1 (1978).
[2] M. Decroux, P. Selvam, J. Cors, B. Seeber, Ø. Fischer, R. Chevrel, P. Rabiller, and M. Sergent, IEEE Trans. Appl. Supercond. **3**, 1502 (1993).
[3] S. Even-Boudjada, V. Tranchant, R. Chevrel, M. Sergent, M. Crosnier-Lopez, Y. Laligant, R. Retoux, and M. Decroux, Mater. Lett. **38**, 90 (1999).
[4] W. Schauer and W. Schelb, IEEE Trans. Magn. **17**, 374 (1981).
[5] D. Dew-Hughes, Philos. Mag. **30**, 293 (1974).
[6] D. Dew-Hughes, Philos. Mag. B **55**, 459 (1987).
[7] H. D. Ramsbottom and D. P. Hampshire, Physica C **274**, 295 (1997).
[8] A. Gumbel, J. Eckert, G. Fuchs, K. Nenkov, K. H. Müller, and L. Schultz, Appl. Phys. Lett. **80**, 2725 (2002).
[9] M. Rikel, IEEE Trans. Appl. Supercond. **9**, 1735 (1999).
[10] D. C. Larbalestier, L. D. Cooley, M. O. Rikel, A. A. Polyanskii, J. Jiang, S. Patnaik, X. Y. Cai, D. M. Feldmann, A. Gurevich, A. A. Squitieri, M. T. Naus, C. B. Eom, E. E. Hellstrom, R. J. Cava, K. A. Regan, N. Rogado, M. A. Hayward, T. He, J. S. Slusky, P. Khalifah, K. Inumaru, and M. Haas, Nature (London) **410**, 186 (2001).
[11] H. Gleiter, Acta Mater. **48**, 1 (2000).
[12] Z. F. Dong, K. Lu, and I. Bakonyi, Nanostruct. Mater. **11**, 187 (1999).
[13] C. C. Koch, Nanostruct. Mater. **2**, 109 (1993).
[14] H. J. Fecht, Nanostruct. Mater. **6**, 32 (1995).
[15] F. Ye and K. Lu, Phys. Rev. B **60**, 7018 (1999).
[16] H. Niu and D. P. Hampshire, Phys. Rev. Lett. **91**, 027002 (2003).
[17] W. A. Fietz and W. W. Webb, Phys. Rev. **178**, 657 (1969).
[18] R. G. Hampshire and M. T. Taylor, J. Phys. F: Met. Phys. **2**, 89 (1972).
[19] D. N. Zheng, H. D. Ramsbottom, and D. P. Hampshire, Phys. Rev. B **52**, 12 931 (1995).
[20] S. A. Keys and D. P. Hampshire, Supercond. Sci. Technol. **16**, 1097 (2003).
[21] H. J. Niu, N. A. Morley, and D. P. Hampshire, IEEE Trans. Appl. Supercond. **11**, 3619 (2001).
[22] X. D. Liu, H. Y. Zhang, K. Lu, and Q. Hu, J. Phys.: Condens. Matter **6**, L497 (1994).
[23] H. J. Niu and D. P. Hampshire, Physica C **372**, 1145 (2002).
[24] L. Ledig, D. Hough, C.-G. Oertel, J. Eckert, and W. Skrotzki, J. Alloys Compd. **285**, 27 (1999).
[25] A. Revesz, J. Lendvai, and I. Bakonyi, Nanostruct. Mater. **11**, 1351 (1999).
[26] S. Even-Boudjada, L. Burel, R. Chevrel, and M. Sergent, Mater. Res. Bull. **33**, 237 (1998).
[27] G. Ziegler, Powder Metall. Int. **10**, 70 (1978).
[28] N. R. Leigh, Ph.D. thesis, *Department of Physics*, University of Durham, Durham, 2001, p. 146.
[29] D. Mandrus, L. Forro, C. Kendziora, and L. Mihaly, Phys. Rev. B **44**, 2418 (1991).
[30] D. R. Harshman and A. P. Mills, Jr., Phys. Rev. B **45**, 10 684 (1992).
[31] S. S. Laderman, R. C. Taber, R. D. Jacowitz, and J. L. Moll, Phys. Rev. B **43**, 2922 (1991).
[32] D. W. Capone II, R. P. Guertin, S. Foner, D. G. Hinks, and H.-C. Li, Phys. Rev. Lett. **51**, 601 (1983).
[33] A. Poddar, P. Mandal, A. N. Das, and B. Ghosh, Phys. Rev. B **44**, 2757 (1991).
[34] J. E. Crow, M. Strongin, R. S. Thompson, and O. F. Kammerer, Phys. Lett. **30A**, 161 (1969).
[35] M. Wagner, Phys. Rev. B **45**, 635 (1992).
[36] M. Suenaga, D. O. Welch, R. L. Sabatini, O. F. Kammerer, and S. Okuda, J. Appl. Phys. **59**, 840 (1986).
[37] Y. J. Uemura, L. P. Le, G. M. Luke, B. J. Sterlieb, W. D. Wu, J. H. Brewer, T. M. Riseman, C. L. Seaman, M. B. Maple, M. Ishikawa, D. G. Hinks, J. D. Jorgensen, G. Saito, and H. Yamochi, Phys. Rev. Lett. **66**, 2665 (1991).
[38] D. P. Hampshire, in *Handbook of Superconducting Materials*, edited by D. Cardwell and D. Ginley (IOP, Bristol, U.K. 2002), p. 1903.
[39] F. Marsiglio and J. P. Carbotte, Phys. Rev. B **33**, 6141 (1986).
[40] M. Furuyama, N. Kobayashi, and Y. Muto, Phys. Rev. B **40**, 4344 (1989).
[41] N. E. Alekseevskii, G. Wolf, S. Krautz, and V. I. Tsebro, J. Low Temp. Phys. **28**, 381 (1977).
[42] H. P. van der Meulen, J. A. A. J. Perenboom, T. T. J. M. Berendschot, J. Cors, M. Decroux, and Ø. Fischer, Physica B **211**, 269 (1995).
[43] N. R. Leigh (Ref. 28), p. 143.
[44] A. Muhlratzer, B. Nickl, B. Seeber, and H. Sprenger, Solid State Commun. **19**, 239 (1976).
[45] C. P. Bean, Rev. Mod. Phys. **36**, 31 (1964).
[46] C. Rossel and Ø. Fischer, J. Phys. F: Met. Phys. **14**, 455 (1984).
[47] S. A. Keys, N. Koizumi, and D. P. Hampshire, Supercond. Sci. Technol. **15**, 991 (2002).
[48] E. J. Kramer, J. Appl. Phys. **44**, 1360 (1973).
[49] E. J. Kramer, J. Electron. Mater. **4**, 839 (1975).
[50] N. Cheggour, M. Decroux, Ø. Fischer, and D. P. Hampshire, J. Appl. Phys. **84**, 2181 (1998).
[51] W. A. Fietz and W. W. Webb, Phys. Rev. **161**, 423 (1967).
[52] D. P. Hampshire and H. Jones, J. Phys. C **21**, 419 (1987).
[53] D. P. Hampshire, Physica C **296**, 153 (1998).
[54] D. P. Hampshire and S.-W. Chan, J. Appl. Phys. **72**, 4220 (1992).
[55] K. Osamura, S. Nonaka, M. Matsui, T. Oku, S. Ochiai, and D. P. Hampshire, J. Appl. Phys. **79**, 7877 (1996).
[56] D. P. Hampshire, in *Applied Superconductivity*, edited by H. C. Freyhardt (DGM Informationsgesellschaft Verlag, Gottingen, 1993), p. 23.
[57] I. J. Daniel and D. P. Hampshire, Phys. Rev. B **61**, 6982 (2000).
[58] A. A. Abrikosov, Sov. Phys. JETP **5**, 1174 (1957).